Some Convergence Considerations in Space-Domain Moment-Method Analysis of a Class of Wide-Band Microstrip Antennas

Deb Chatterjee, *Member, IEEE,* and Richard G. Plumb, *Senior Member, IEEE*

***Abstract*—The method of moments (MoM) analysis of probe-fed rectangular microstrip patches requires the inclusion of a probe-to-patch attachment mode-expansion function when the substrate thickness $d \geq 0.02\lambda$, where λ is the free-space wavelength. The results for the input impedance showed increased divergence with measurements when the attachment mode was omitted from the full-wave analysis. The attachment mode can be expressed as an infinite eigenfunction series that increases the *fill time* of the impedance matrix in an MoM analysis. In an earlier investigation, the infinite eigenfunction series was reduced to a residue series that required one or two terms compared to about 55 terms for the eigenfunction series. In this paper, the convergence properties of the eigenfunction and residue series are investigated in view of rigorous MoM analysis. The relative errors resulting from replacing the eigenfunction by the residue series for the attachment mode, are compared by numerically evaluating a class of two-dimensional (2-D) spatial integrals shown to be closely related to the elements of an MoM impedance matrix. Additionally, the computation times for the evaluation of these integrals for the two forms of the attachment mode-expansion function are also included. Based on the superior convergence properties of the residue series for the attachment mode-expansion function, it is mathematically justified that this form can readily be used for analytic reduction of the spatial, reaction integrals from four to 2-D forms. This feature allows further reduction of the fill time of the MoM impedance matrix, suggesting the possibility of developing an efficient space-domain MoM technique for modeling of wide-band microstrip antennas.**

***Index Terms*—Method of moments, microstrip antennas.**

I. Introduction

USE of small microstrip antennas with probe feeds is becoming increasingly popular for handheld personal communication systems (PCS) cellphones [1]. Broad-band antennas are desired [2] and computer-aided design tools for broad-band probe-fed patches are thus attracting attention [3], [4]. The effect of the probe location (at the high-frequency end of the stipulated bandwidth) on the input impedance is thus critical. The input impedance variation with frequency dictates the wide-band properties of such microstrip antennas for PCS applications ([1, fig. 2]). While approximate modeling techniques such as transmission line or cavity models [4] can be used to compute the input impedance, it is desirable to employ full wave analysis techniques [3] for optimizing designs that are initiated using the approximate methods. Since input impedance calculation is central to modeling wide-band antennas, full wave analysis plays a critical role in such problems.

It has recently been emphasized in [5] that full wave modeling of broad-band antennas is essential for realizing many novel designs. However, as discussed in [4], such full wave models require prohibitive computational resources and, hence, efficient modeling techniques are sought that lead to reduced storage requirements and/or faster processing speeds. Either feature is an important consideration for full wave performance analysis of wide-band antennas [5]. The subject of this paper is to explore methods for developing efficient computer models for full wave characterization of probe-fed microstrip antennas.

The investigations reported here discuss enhancement of processing speed of a moment-method solution [6] to microstrip antennas. As discussed in [6], moment-method solutions require computation of elements of the voltage and impedance matrices and the bulk of the computation time is spent in filling these matrices. Most of the efficient moment-method solutions therefore aim at reducing the fill time of these matrices by use of special form of the appropriate Green's functions [5], [7]. For microstrip antenna problems the appropriate Green's function contains Sommerfeld integrals and some efficient methods for their computation have been addressed in [8], [9].

For most moment-method solutions to probe-fed microstrip patch antennas, the entire-domain basis functions are used ([3, ch. 1]). The information gleaned from [10], [11] suggests that the spectral-domain moment-method approach is the most common since the relevant Green's functions do not involve the traditional Sommerfeld integrals. However, the individual elements of both voltage and impedance matrices in a spectral-domain moment method will have a Sommerfeld-like behavior [11, eqs. (16)–(20)], necessitating careful attention to their computation. The situation becomes very complicated for the impedance matrix calculations because the source and observer locations are coplanar, resulting in very poor convergence of the spectral integrals. This naturally increases the fill time of the impedance matrix and sophisticated analytical techniques can often help salvage such problems [10].

In contrast with spectral methods, space-domain moment-method techniques have also been used to address mutual coupling problems [12]. Solving mutual coupling problems via the

Manuscript received April 8, 1999; revised October 20, 1999. This work was supported in part by Allied Signal Corporation, Kansas City, MO.

D. Chatterjee is with the Electrical and Computer Engineering Department, University of Missouri-Columbia/Kansas City (UMKC), Kansas City, MO 64110-2499 USA.

R. G. Plumb is with the Electrical Engineering Department, State University of New York (SUNY) at Binghamton, Binghamton, NY 13902 USA.

Publisher Item Identifier S 0018-926X(00)01642-2.

space-domain method appears to be more promising because evaluation of spectral integrals for increased lateral separation between source and observer points becomes formidable due to the rapid oscillation of the integrands. Comparison between space and spectral domain methods for microstrip antennas have been presented in [13] and the closed-form results in [14] were obtained in the space domain for impedance matrix elements. In line with these appropriate references, the primary purpose of this paper is to augment the space-domain method of moments as applied to modeling wide-band probe-fed microstrip patches.

Probe-fed microstrip patch antennas for wide-band PCS applications require modeling the probe feed with the complete moment-method solution. This, following the detailed investigations in [15], was included using an additional attachment mode-expansion function for the patch and feed [16]. The attachment mode-expansion function, first introduced in [17] on the patch, is an infinite eigenfunction series and, for rectangular patch geometries, its derivation can be found in [3, pp. 26–28] from the corresponding cavity model. In [3] and [16], the spectral-domain analysis proceeds by taking the Fourier transform of the attachment mode; the spectral integrals were evaluated numerically via standard techniques [18], [19], as shown in [10] and [11].

In [20], the infinite eigenfunction series was analytically reduced to a residue series form for a rectangular patch. It was shown in [20] that only one or two terms of the residue series are numerically adequate compared to about 55 terms of the eigenfunction series. In view of the investigation in [20], some preliminary results for convergence properties were presented in [21], [22] using the residue series for the attachment mode. This paper examines the problem more completely and detailed comparisons are presented here using the residue and eigenfunction series forms. However, due to the nature of the formulation of the probe-to-patch attachment mode [3], [16], [20], all the discussions are limited to rectangular microstrip patches only.

In Section II the important aspects of the space-domain formulation are summarized from [22]. In Section III detailed numerical results for establishing the convergence properties of the space-domain method are included. The main emphasis of this paper are these results, which makes this work distinct from [21] and [22]. This is followed by conclusions and references.

II. Summary of Spatial-Domain Formulation

The geometry of the problem is shown in Fig. 1. The total current on the patch is written as

$$\begin{aligned}\vec{\mathbf{J}}_{\text{patch}}(x,y) &= \hat{\mathbf{x}}\mathcal{I}^{x}_{\text{att}}\Phi^{x}_{\text{att}}(x,y) + \hat{\mathbf{y}}\mathcal{I}^{y}_{\text{att}}\Phi^{y}_{\text{att}}(x,y) \\ &\quad + \hat{\mathbf{x}}\sum_{m=1}^{M}\mathcal{I}^{m}_{x\,\text{edb}}\Psi^{m}_{x\,\text{edb}}(x,y) \\ &\quad + \hat{\mathbf{y}}\sum_{n=1}^{N}\mathcal{I}^{n}_{y\,\text{edb}}\Psi^{n}_{y\,\text{edb}}(x,y). \end{aligned} \tag{1}$$

In (1) $\mathcal{I}^{x,y}_{\text{att}}$ and $\mathcal{I}^{m,n}_{x\,\text{edb},y\,\text{edb}}$ are the unknown complex (scalar) amplitudes of the x and y components of the attachment and entire-domain basis functions, respectively. The superscripts m,n stand for the mth and nth entire-domain modes. The expansion functions $\Phi^{x,y}_{\text{att}}(x,y)$ and $\Psi^{m,n}_{x\,\text{edb},y\,\text{edb}}(x,y)$ are designated as vectors in (1) and their support is $\Lambda : (-L/2) \le x \le (+L/2)$ and $(-W/2) \le y \le (+W/2)$. Formulating a moment-method solution [3], [6], [16], one obtains the matrix equation

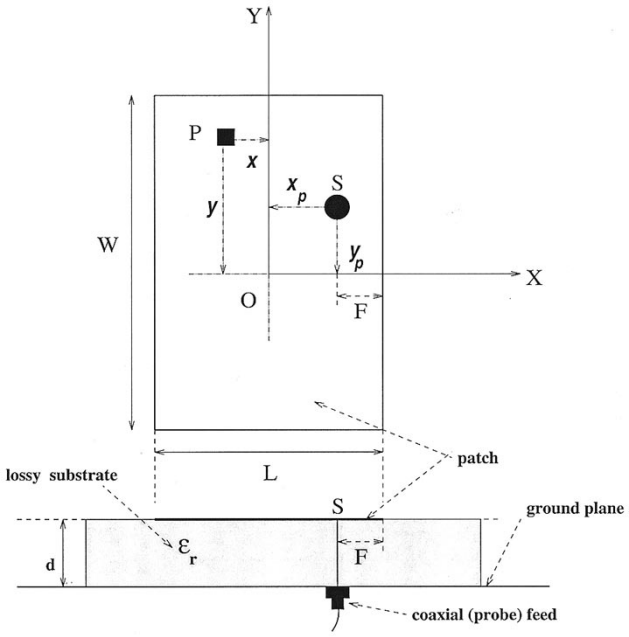

Fig. 1. Cross-sectional views of a rectangular microstrip antenna. The point **P** is an arbitrary point on the patch and **S** is the probe-to-patch junction.

$$[V] = [Z] \cdot [I]. \tag{2}$$

The main focus of this presentation is on the impedance matrix on the immediate right side of (2).

With a slight change of notation, the eigenfunction series for the attachment mode-expansion functions $\Phi^{(x,y)E}_{\text{att}}(x,y)$ can be obtained from [16] and [3, p. 28, eqs. (1.155)–(1.158)]. These read

$$\begin{aligned}\Phi^{xE}_{\text{att}}(x,y) &= \sum_{m=0}^{\infty}\mathcal{K}^{x}_{E}(m,y_p) \\ &\quad \times \cos\Big(\frac{m\pi}{2} + \frac{m\pi y}{W}\Big)\mathcal{F}_s(x,x_p;m)\end{aligned} \tag{3}$$

and

$$\begin{aligned}\Phi^{yE}_{\text{att}}(x,y) &= \sum_{m=0}^{\infty}\mathcal{K}^{y}_{E}(m,y_p) \\ &\quad \times \sin\Big(\frac{m\pi}{2} + \frac{m\pi y}{W}\Big)\mathcal{F}_c(x,x_p;m)\end{aligned} \tag{4}$$

for the x and y components of the attachment modes, respectively. In (3) and (4), x_p and y_p indicate the probe location in Fig. 1. The coordinates of the location of an arbitrary point P are also shown there. The superscript or subscript E in (3) and (4) designates that these are eigenfunction series. The quantities $\mathcal{K}^{x,y}_{E}(m,y_p)$ can be interpreted as modal amplitudes associated with each of the integers m and are taken as constants for the remainder of the paper. Their explicit forms can be found in [3] and [16] and are omitted here for brevity. Similar remarks apply

to the functions $\mathcal{F}_{c,s}(x, x_p; m)$, which contain simple trigonometric functions.

The two-term residue series, designated by superscript R, can be obtained from [20, eqs. (39)–(47)]

$$\begin{aligned}\Phi_{\text{att}}^{xR}(x,y) &= \mathcal{K}_1^{xR}(x_p,y_p,\nu_1)\cos\left(\frac{\pi x}{L}\right)\cos\left(\frac{\nu_1\pi}{2}-\frac{\nu_1\pi|y|}{W}\right)\\ &\quad+\mathcal{K}_2^{xR}(x_p,y_p,\nu_2)\sin\left(\frac{2\pi x}{L}\right)\\ &\quad\times\cos\left(\frac{\nu_2\pi}{2}-\frac{\nu_2\pi|y|}{W}\right)\end{aligned} \tag{5}$$

for the x component and from [20, eq. (54)]

$$\begin{aligned}\Phi_{\text{att}}^{yR}(x,y) &= \mathcal{K}_1^{yR}(\nu_0)[\sin(\nu_0\alpha_1)\mp\sin(\nu_0[\pi-|\alpha_2|])]\\ &\quad+\mathcal{K}_2^{yR}(\nu_1,x_p)\sin\left(\frac{\pi x}{L}\right)\\ &\quad\times[\sin(\nu_1\alpha_1)\mp\sin(\nu_1[\pi-|\alpha_2|])]\end{aligned} \tag{6}$$

for the y component, respectively. The complex quantities $\mathcal{K}_{1,2}^{xR}(x_p,y_p,\nu_1)$ and $\mathcal{K}_{1,2}^{yR}(x_p,\nu_{0,1})$ can be obtained from [20] and are treated as constants throughout this paper. These depend on the geometry of the patch and the frequency and are omitted here for brevity. The quantities

$$\alpha_{1,2}=\frac{\pi(y\pm y_p)}{W} \tag{7}$$

in (6) and the $\pm$ signs are chosen for subscripts 1 and 2, respectively, with $\alpha_1>0(-)$ and $\alpha_2<0(+)$.

Next, we focus on the calculation of the inner products of the impedance matrix elements in (2). To illustrate the convergence issues, it suffices to consider the self-terms of the impedance matrix due to the x and y components of the attachment mode-expansion function. The conclusions apply equally well to the various mutual (or off-diagonal) terms.

To that end, the inner product

$$\begin{aligned}-\langle\overline{\overline{\mathcal{L}}}_H(\vec{\Phi}_{\text{att}}^{xE}),\vec{\Phi}_{\text{att}}^{xE}\rangle|_\Lambda &= \int_{-\frac{W}{2}}^{+\frac{W}{2}}\int_{-\frac{W}{2}}^{+\frac{W}{2}}\int_{-\frac{L}{2}}^{+\frac{L}{2}}\int_{-\frac{L}{2}}^{+\frac{L}{2}}dy\,dy'\,dx\,dx'\\ &\quad\times G_{xx}(\rho)\Phi_{\text{att}}^{xE}(x,y)\Phi_{\text{att}}^{xE}(x',y')\end{aligned} \tag{8}$$

for the x component and

$$\begin{aligned}-\langle\overline{\overline{\mathcal{L}}}_H(\vec{\Phi}_{\text{att}}^{yE}),\vec{\Phi}_{\text{att}}^{yE}\rangle|_\Lambda &= \int_{-\frac{W}{2}}^{+\frac{W}{2}}\int_{-\frac{W}{2}}^{+\frac{W}{2}}\int_{-\frac{L}{2}}^{+\frac{L}{2}}\int_{-\frac{L}{2}}^{+\frac{L}{2}}dy\,dy'\,dx\,dx'\\ &\quad\times G_{yy}(\rho)\Phi_{\text{att}}^{yE}(x,y)\Phi_{\text{att}}^{yE}(x',y')\end{aligned} \tag{9}$$

for the y component of the attachment mode can be obtained via use of (3) and (4), respectively. In (8) and (9), the primes indicate operations with respect to source coordinates. The lateral separation between the source and field points on the interface is defined via $\rho=\sqrt{(x-x')^2+(y-y')^2}$ in (8) and (9). From [8, eqs. (6), (10)] one finds

$$G_{xx}(x-x';y-y')\equiv G_{xx}(\rho)=\frac{-\jmath}{2\pi k_0^2}\left[k_0^2U+\frac{\partial^2P}{\partial x^2}\right] \tag{10}$$

and

$$G_{yy}(x-x';y-y')\equiv G_{yy}(\rho)=\frac{-\jmath}{2\pi k_0^2}\left[k_0^2U+\frac{\partial^2P}{\partial y^2}\right]. \tag{11}$$

In (10) and (11), the U and P are Sommerfeld integrals and are functions of ρ. The mathematically formidable nature of (8) and (9) suggests that the fill time for the impedance matrix in (2) can be a serious problem.

In a similar manner, one can evaluate the inner products for the two-term residue series for the attachment mode. Use of (5) gives

$$\begin{aligned}-\langle\overline{\overline{\mathcal{L}}}_H(\vec{\Phi}_{\text{att}}^{xR}),\vec{\Phi}_{\text{att}}^{xR}\rangle|_\Lambda &= \int_{-\frac{W}{2}}^{+\frac{W}{2}}\int_{-\frac{W}{2}}^{+\frac{W}{2}}\int_{-\frac{L}{2}}^{+\frac{L}{2}}\int_{-\frac{L}{2}}^{+\frac{L}{2}}dy\,dy'\,dx\,dx'\\ &\quad\times G_{xx}(\rho)\Phi_{\text{att}}^{xR}(x,y)\Phi_{\text{att}}^{xR}(x',y').\end{aligned} \tag{12}$$

Similarly, via direct substitution from (6), one can obtain an expression similar to (12) for the inner product

$$\begin{aligned}-\langle\overline{\overline{\mathcal{L}}}_H(\vec{\Phi}_{\text{att}}^{yR}),\vec{\Phi}_{\text{att}}^{yR}\rangle|_\Lambda &= \int_{-\frac{W}{2}}^{+\frac{W}{2}}\int_{-\frac{W}{2}}^{+\frac{W}{2}}\int_{-\frac{L}{2}}^{+\frac{L}{2}}\int_{-\frac{L}{2}}^{+\frac{L}{2}}dy\,dy'\,dx\,dx'\\ &\quad\times G_{yy}(\rho)\Phi_{\text{att}}^{yR}(x,y)\Phi_{\text{att}}^{yR}(x',y').\end{aligned} \tag{13}$$

The foregoing analysis indicates that employing the eigenfunction series in (3) and (4) for the attachment mode to (8) and (9) results in a dual infinite series of fourfold integrals. Since many such terms, which have been omitted here, shall actually be present in the full expansion of (8) and (9), their computation is thus very costly. It follows from (5) and (6) that the full expansion of the inner products in (12) and (13) will contain a *finite* number of terms.

Regardless of the nature (exact [9] or asymptotic [8]) of the Sommerfeld integrals, one can employ the integration-by-parts procedure with the inner products in (8), (9), (12), and (13) to transfer the second derivatives in (10) and (11) over to the expansion functions. It has been shown in [13] that such a procedure may be extended to expansion functions with finite discontinuities, but it is mathematically preferable to perform this operation on expansion functions that are well behaved over the entire support region.

To that end, examining the results in [20, figs. 4–6] and Fig. 2, it follows that if the effects of the junction discontinuity are numerically insignificant in the calculation of the inner products, then an efficient method of calculating the impedance matrix elements can be developed using (5) and (6) instead of (3) and (4). Additionally the fourfold integrals in (8), (9), (12), and (13), can be further reduced to double integrals following the mapping

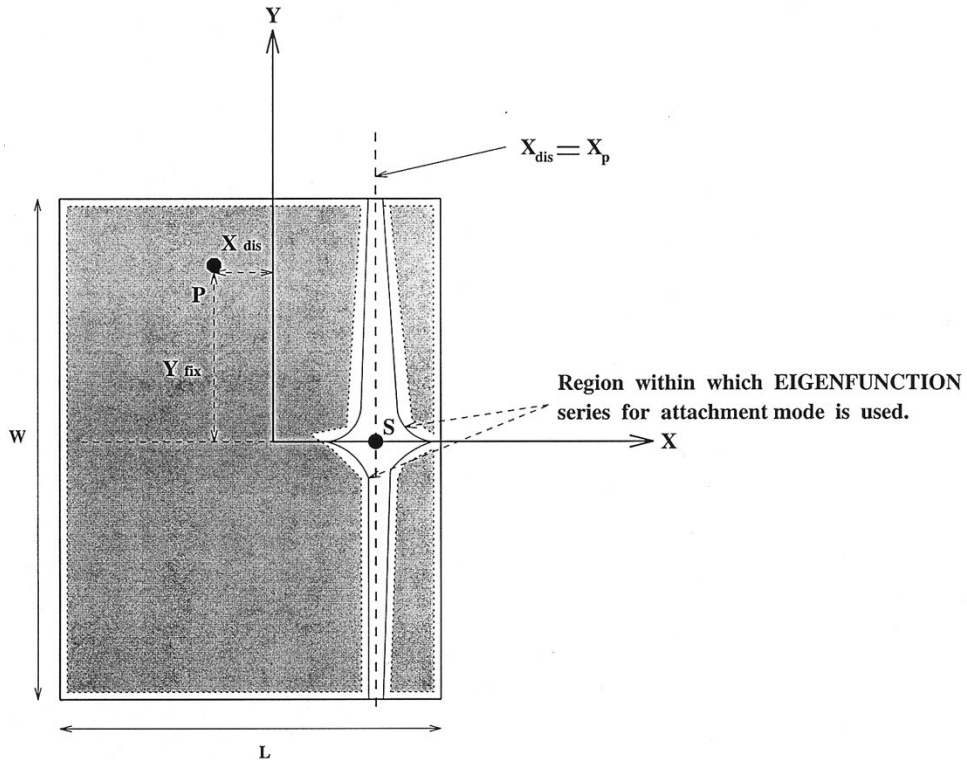

Fig. 2. Regions of validity of residue and eigenfunction series.

technique in [12] and depicted pictorially in Fig. 3. Following [12], [13], and [22] the integration-by-parts method is used to eliminate the second derivatives in (10) and (11) in the inner products of (8) and (9). This procedure is somewhat complicated to justify for the eigenfunction series for the probe-to-patch attachment mode that contains sharp discontinuities in the close vicinity of the probe-to-patch junction. For the residue series, which is smoothly varying at the junction, the application of the same procedure is mathematically straightforward.

The preceding observations underscore the need for examining the convergence issues. Summarizing, we note that the *fill time* for the $[Z]$ matrix in (2) can be reduced if two independent constraints are satisfied simultaneously. This means that:

1) one- or two-term residue series can be used in evaluating the impedance matrix inner products instead of the truncated infinite eigenfunction series, implying use of (12) and (13) instead of (8) and (9), respectively;
2) the analytic reduction of fourfold to twofold integrals will be possible via the coordinate transformation method shown in Fig. 3; the residue series in (5) and (6) are mathematically similar in form to the entire-domain basis functions [13] for a single rectangular patch and are easily amenable to such manipulations.

Constraints 1) and 2) are satisfied by the residue series form for the attachment mode. However, prior to the analytical reduction described in 2), it is necessary to show numerically that the residue series form satisfies constraint 1).

The closed-form evaluation in Fig. 3 works only for rectangular patches and apertures because the expansion functions are a superposition of sines and cosines that can be integrated in closed form over the finite size of the patch. For circular

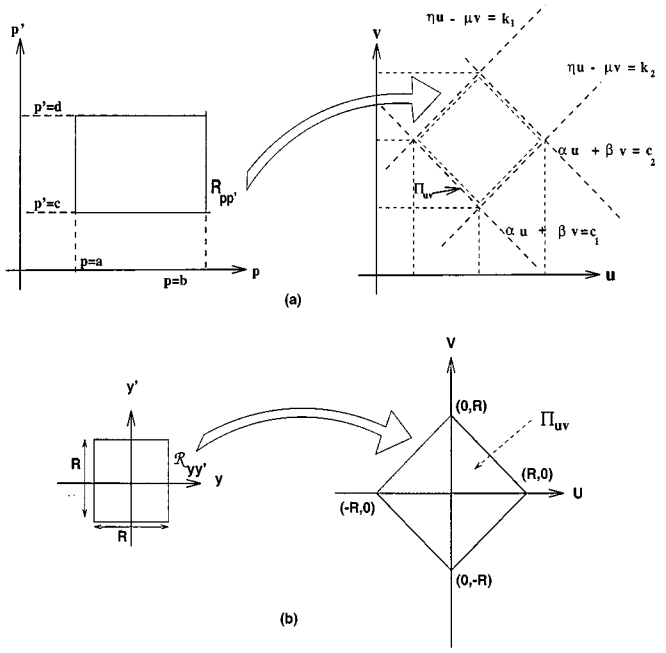

Fig. 3. (a) Linear mappings from $p - p'$ to $u - v$ planes. (b) $\mathcal{R}_{yy'} \rightarrow \Pi_{uv}$ is a special case of (a) and $\Pi_{uv} = 4\Delta$, where Δ is the area of the shaded triangle in (b). Such mappings often reduce the dimensionality of reaction integrals in space-domain moment-method analysis of electrically large problems [12].

shapes the expansion functions are Bessel functions that cannot be readily integrated in closed form over the finite region of the circular area.

The mapping technique in [13], when applied to reaction integrals for rectangular radiating shapes, reduces the dimension

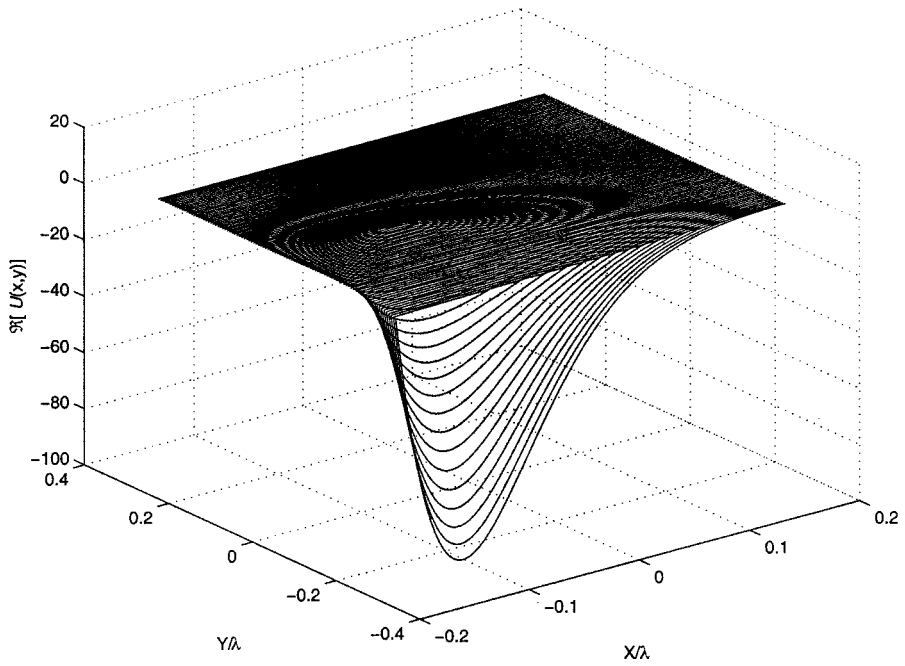

Fig. 4. Three-dimensional plot of the Sommerfeld integrand given in (15).

of the integral by two. Consequently, to establish the superior convergence properties of the residue series, reduced forms for the integrals in (8), (9), (12), and (13) are sought. The underlying hypothesis is that if the convergence properties can be established at a lower order, then the same general properties can be expected to be valid for higher dimension integrals involving the same residue series.

Thus, to develop an efficient space-domain technique, one needs to examine the convergence properties of the twofold canonical integral

$$\mathcal{I}_{\rm att}^{E,R} = \int_{-\frac{W}{2}}^{+\frac{W}{2}} \int_{-\frac{L}{2}}^{+\frac{L}{2}} \mathcal{U}(x,y)\Theta_{\rm att}^{E,R}(x,y)\,dx\,dy \qquad (14)$$

in detail. Such a numerical analysis would also reveal if the effect of the discontinuity is important for full wave analysis applications. In (14), $\mathcal{U}(x,y)$ is a suitably chosen function that exhibits exponentially decaying and oscillatory characteristics. The function $\Theta_{\rm att}^{E,R}(x,y)$ stands for each of the expansion functions in (3)—(6). The eigenfunction series given by (3) and (4) and generically designated by $\Theta_{\rm att}^{E}(x,y)$ has a peak discontinuity at $x = x_p$. The corresponding residue series form given by (5) and (6) and generically designated by $\Theta_{\rm att}^{R}(x,y)$ is smoothly varying at this junction location. The original inner products, when suitably reduced, would comprise a superposition of integrals of the generic form given by (14).

III. Evaluation of Canonical Integral in (14) Using the IMSL Software [18]

The residue and eigenfunction series have been shown in [20] to differ across a narrow strip known as the Stokes region, as shown in Fig. 2. Consequently, it appears practical to evaluate (14) for eigenfunction (3) and (4) and residue (5) and (6) series, respectively. The $\mathcal{U}(x,y)$ in (14) does not in any way lend insight to the convergence behavior of the two forms of the attachment mode-expansion function. Hence, it can be replaced in (14) by (15), shown at the bottom of the page, integrands, which are much simpler to compute. The numerical differences between the eigenfunction and residue series are then defined by

$$\mathcal{R}_{\rm err} = \frac{|\mathcal{I}_{\rm att}^{E} - \mathcal{I}_{\rm att}^{R}|}{|\mathcal{I}_{\rm att}^{E}|} \times 100. \qquad (16)$$

To evaluate (14) numerically, the Institute of Mathematical and Statistical Libraries (IMSL) software package [18] is used. All the calculations were done in double-precision arithmetic. To that end, following [19], the two-dimensional (2-D) integration routine double precision two-dimensional quadrature (DTWODQ) [18]was used to evaluate (14). This routine evaluates double integrals and the IMSL package has its various versions. These various versions of DTWODQ are to be used for various classes of functions or if the function has different behavior over

$$\mathcal{U}(x,y) = \begin{cases} e^{-N(x+y)}\,\frac{\sin(Nx)}{Nx}\,\frac{\sin(Ny)}{Ny} & \text{for Sommerfeld-like or} \\ \dfrac{e^{-\jmath k\rho}}{k\rho} & \text{for free-space Green's function} \end{cases} \qquad (15)$$

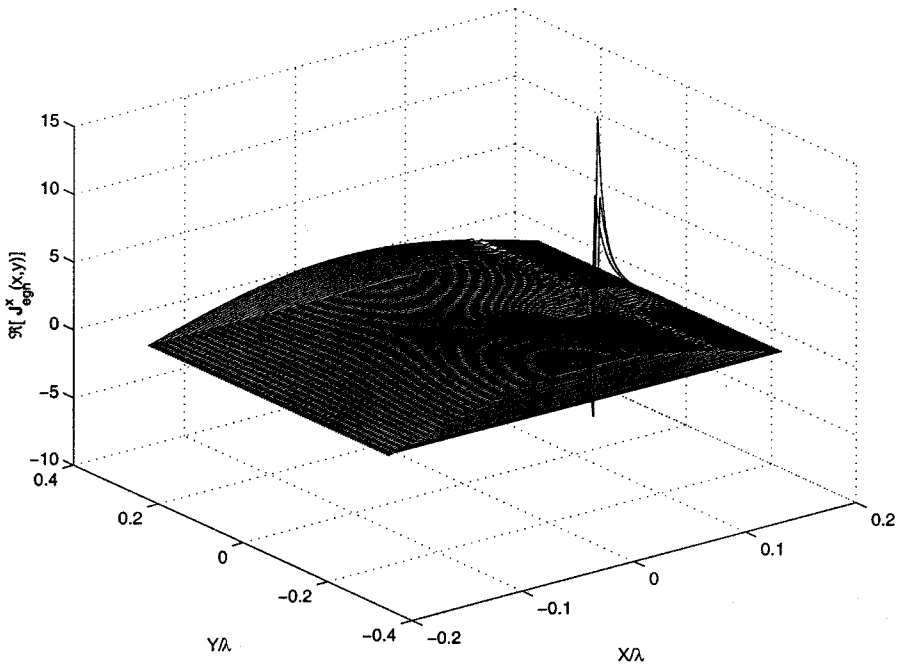

Fig. 5. Three-dimensional plot of the x component of the attachment mode for 55 terms in (3).

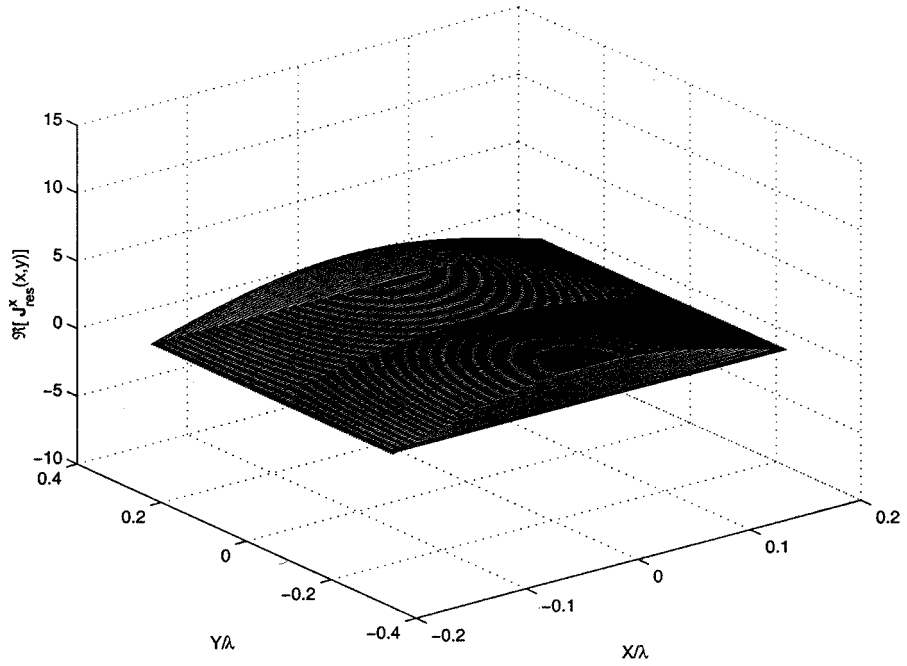

Fig. 6. Three-dimensional plot of the x component of the attachment mode for the two-term expression in (5).

different regions in the range of integration. Recalling the discontinuous nature of $\Theta^E_{\rm att}(x,y)$ (eigenfunction series) from Fig. 2, it is possible to write

$$\mathcal{I}^E_{\rm att} = \int_{-\frac{W}{2}}^{+\frac{W}{2}} dy \left\{ \int_{-\frac{L}{2}}^{x_p-\Delta} \mathcal{U}(x,y)\Theta^E_{\rm att}(x,y)\,dx + \int_{x_p-\Delta}^{x_p+\Delta} \mathcal{U}(x,y)\Theta^E_{\rm att}(x,y)\,dx + \int_{x_p+\Delta}^{+\frac{L}{2}} \mathcal{U}(x,y)\Theta^E_{\rm att}(x,y)\,dx \right\} \quad (17)$$

for the eigenfunction form. The smooth behavior of the residue series allows one to write

$$\mathcal{I}^R_{\rm att} = \int_{-\frac{W}{2}}^{+\frac{W}{2}} \int_{-\frac{L}{2}}^{+\frac{L}{2}} \mathcal{U}(x,y)\Theta^R_{\rm att}(x,y)\,dx\,dy. \quad (18)$$

The width of the narrow strip can be approximated by 2Δ, where $\Delta = 2.0 \times 10^{-02}\lambda$ was chosen from ([20, fig. 5(b)]. To use the DTWODQ routine in the IMSL package, the input parameters were set to $\mathrm{ERRABS} = 1.0 \times 10.0^{-10}$ (absolute error) and

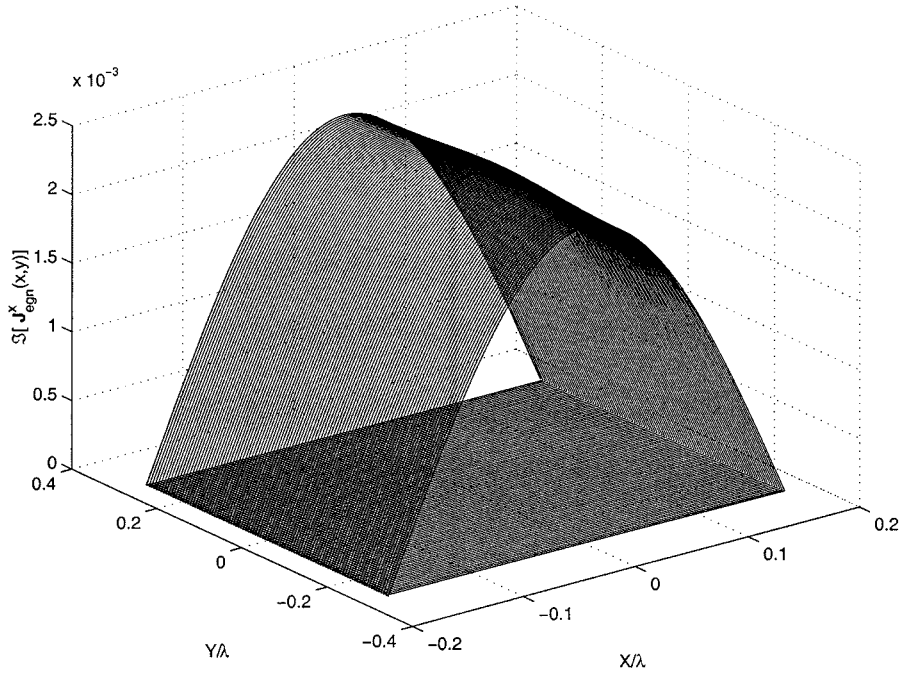

Fig. 7. Three-dimensional plot of the x component of the attachment mode for 55 terms in (3).

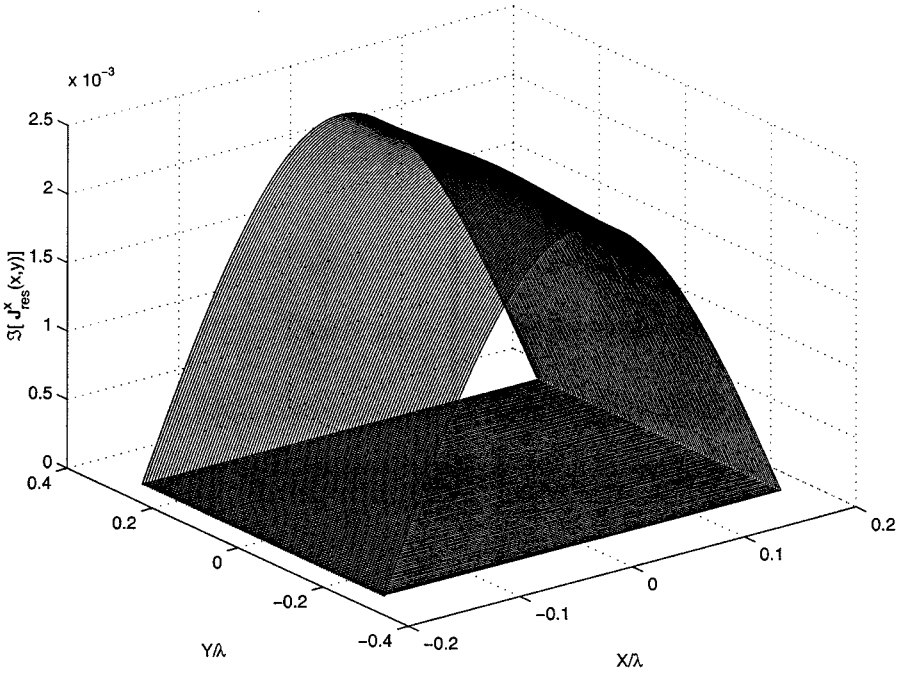

Fig. 8. Three-dimensional plot of the x component of the attachment mode for the two-term expression in (5).

$\mathrm{ERRREL} = 1.0 \times 10.0^{-10}$ (relative error). Outside $x_p - \Delta \leq x \leq x_p + \Delta$, there are no discontinuities in the attachment mode and, hence, one can set $\mathrm{IRULE} = 6$ to define the oscillatory nature of the integrand in (17). Within the narrow region (second term in (17)), $\mathrm{IRULE} = 1$ was set to specify that the function has a peak discontinuity. For (18) $\mathrm{IRULE} = 6$ was used throughout the entire range of integration. The program was run in a time-sharing (batch) mode and an approximate estimate of the central processing unit (cpu) time was obtained. Thus, for every run the result for (16) and the corresponding approximate cpu times were obtained by varying the number of terms in the eigenfunction series. The results are discussed in the next section.

IV. Discussion of Results

The results of this investigation are shown in Figs. 4–18. These results refer to the single-patch geometry chosen from

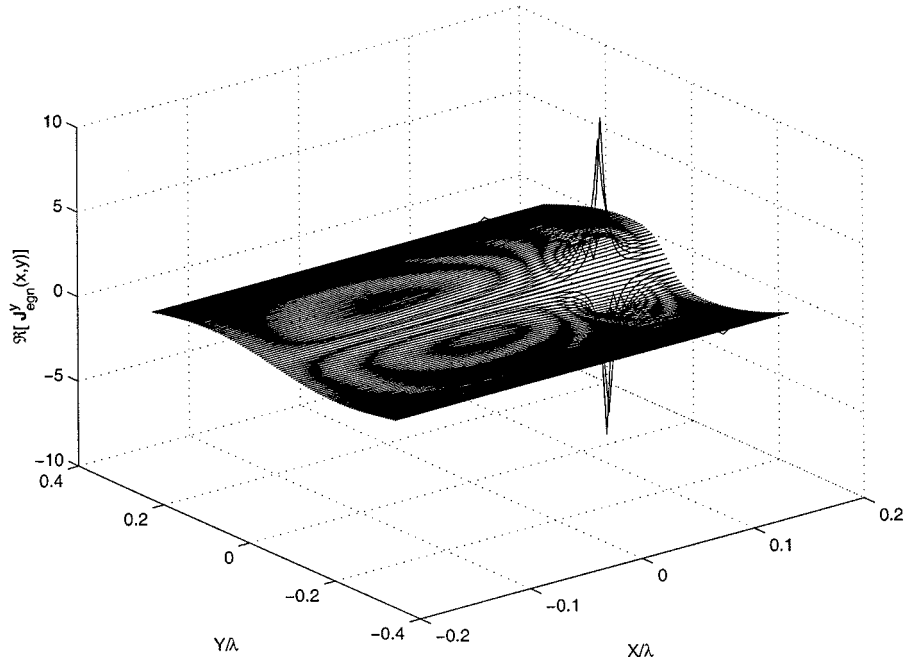

Fig. 9. Three-dimensional plot of the y component of the attachment mode for 55 terms in (4).

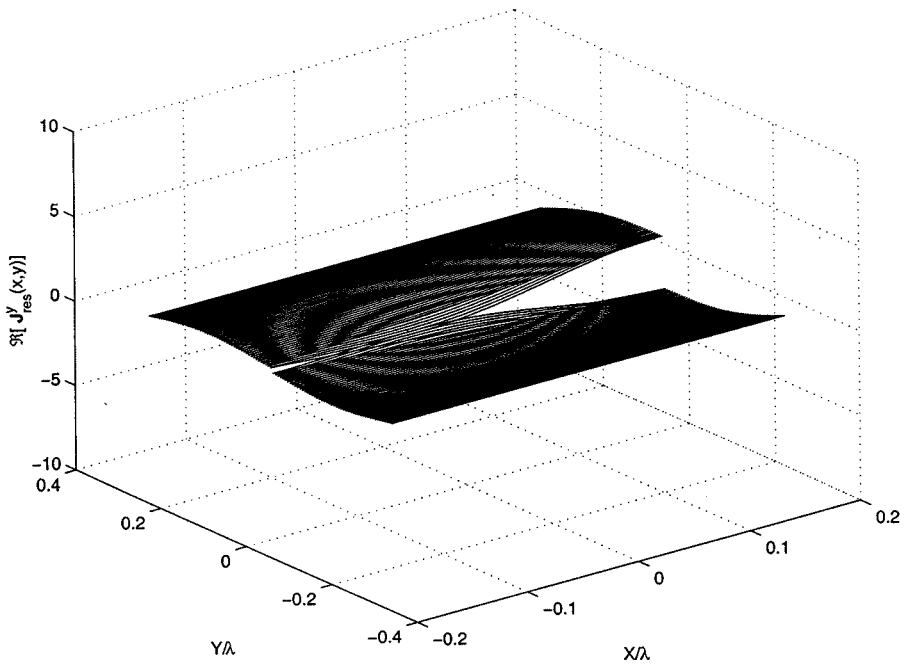

Fig. 10. Three-dimensional plot of the y component of the attachment mode for the two-term expression in(6).

[15, patch #6b]. Referring to Fig. 1, $W = 2.0$, $L = 1.25$, $Xp = 0.425$, and $Yp = 0.0$, all in centimeters and the measured resonant frequency $f = 7.65$ GHz. The substrate has the relative permittivity $\epsilon_r = 2.22(1 - j0.0001)$. In [15, fig. 8] the measured input impedance data are shown for $f = 7.3$ to 8.5 GHz for this specific patch geometry. This range of frequencies corresponds to an instantaneous bandwidth of approximately 16%. The results for other patch geometries in [15] were also obtained, but are omitted here due the repetitive nature of these results. The important results that demonstrate the convergence properties are shown in Figs. 13–18. Since these results refer to the computation of $\mathcal{R}_{\rm err}$ in (16), additional results related to the integrands in (17) and (18) are included in Figs. 4–12. These results show the nature of the integrands over the entire support regions defined by $(-L/2) \leq x \leq (+L/2)$ and $(-W/2) \leq y \leq (+W/2)$. The data in Figs. 4–12 were generated for 100×100 sample points over the entire patch area and at the frequency, $f = 8.5$ GHz. Other necessary information is included in the respective figures themselves and, hence, is not repeated here. In Figs. 4–18, $\Re(\cdots)$ and $\Im(\cdots)$ stand for

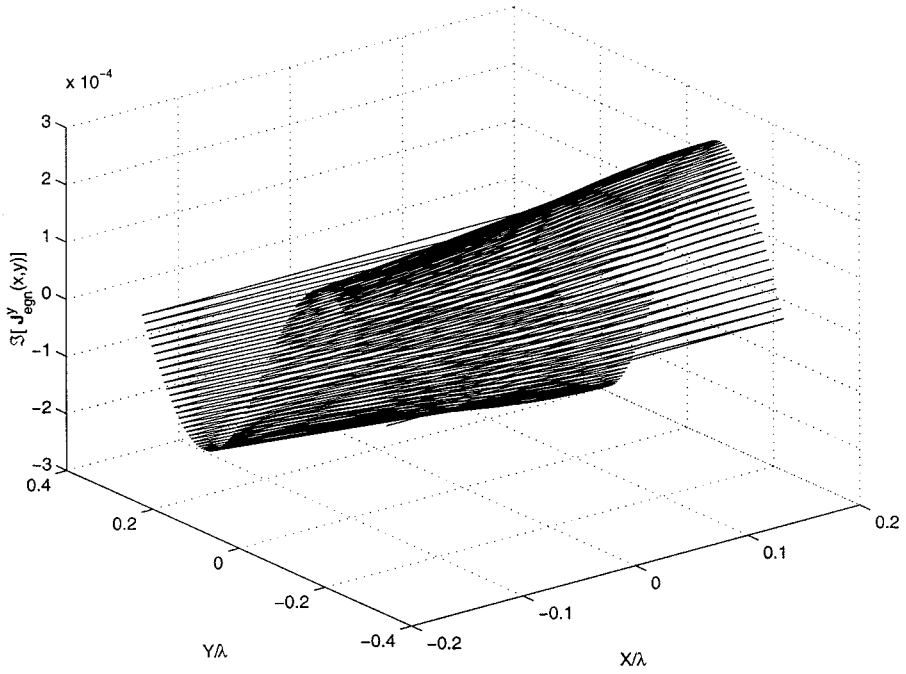

Fig. 11. Three-dimensional plot of the y component of the attachment mode for 55 terms in (4).

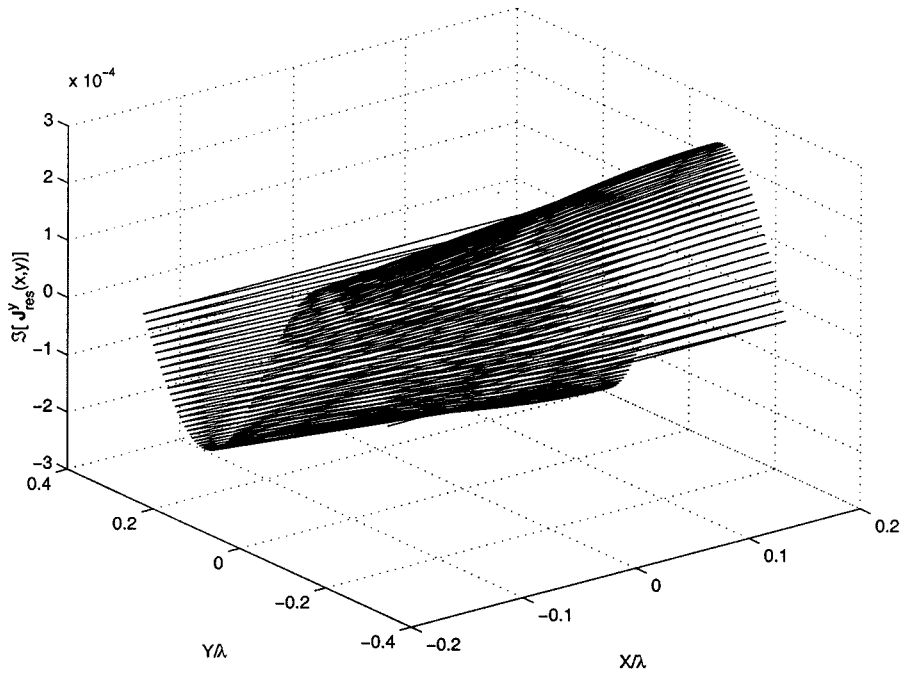

Fig. 12. Three-dimensional plot of the y component of the attachment mode for the two-term expression in (6).

real and *imaginary* parts of $(\cdots)$, respectively. In these figures, $\mathbf{J}_{\mathrm{egn}}^{(x,y)}(x,y)$ stand for the corresponding eigenfunction expansion functions for the x- and y-components in (3) and (4), respectively. Similarly, $\mathbf{J}_{\mathrm{res}}^{(x,y)}(x,y)$ stand for the corresponding residue series expansion functions for the x- and y-components in (5) and (6), respectively. The computations were carried out at the University of Kansas Academic Computing Services, DEC AlphaServer 1000A machine with an open VMS Alpha version 7.2.1 operating system. These results are briefly discussed below.

In Fig. 4, the nature of the Sommerfeld integrand, defined via (15), is shown. These data refer to a degree of oscillation $N = 10$. Only the real part is shown, as the imaginary part is redundant since all the other parameters for $\mathcal{U}(x,y)$ are real. Figs. 5–8 compare the nature of the x component of the attachment mode-expansion function given by (3) and (5). It is

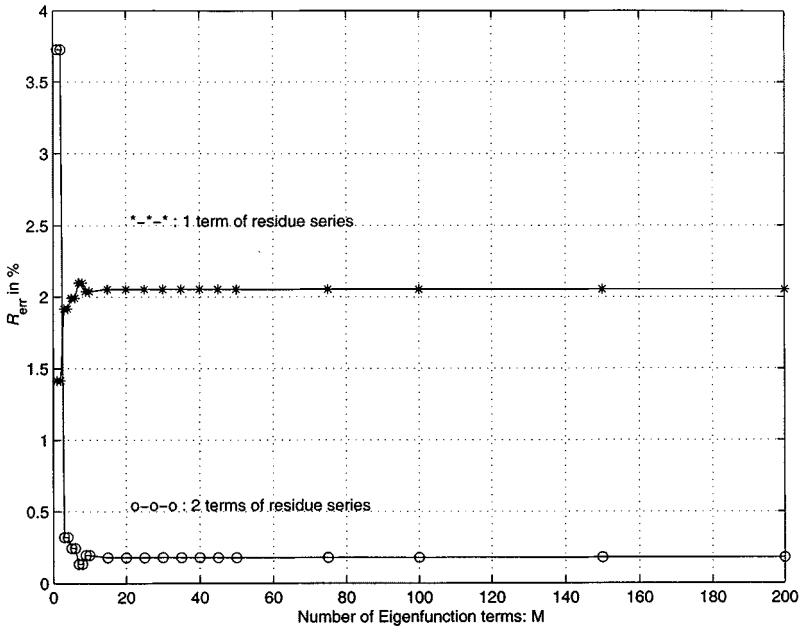

Fig. 13. Comparisons of $\mathcal{R}_{\rm crr}$ for x component of the attachment mode at $f = 8.5$ GHz.

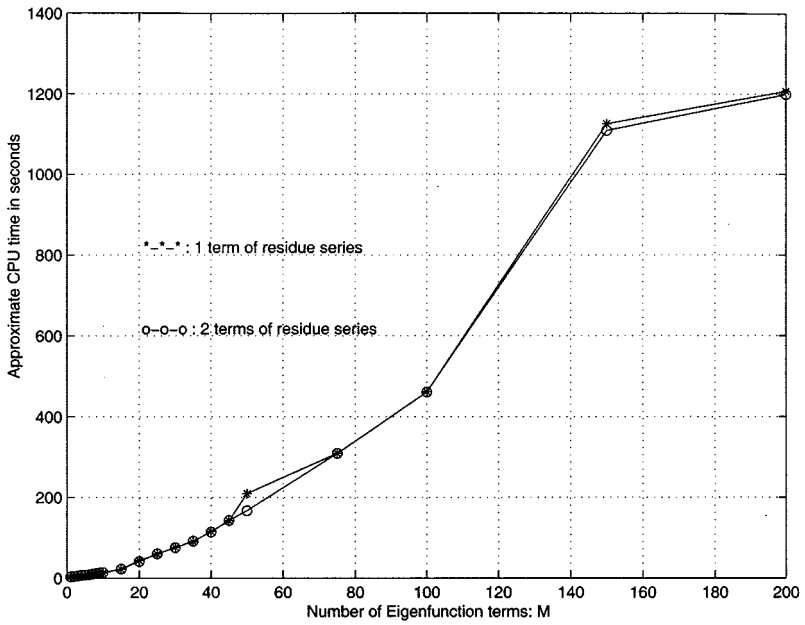

Fig. 14. Computation cost for the x component of the eigenfunction series for the attachment mode at $f = 8.5$ GHz.

obvious that the composite integrand, which is a product of $\mathcal{U}(x, y)$ and $\Phi^{xE}_{\rm att}(x, y)$ (or $\Phi^{xR}_{\rm att}(x, y)$), will be almost the same for $\mathcal{I}^{E}_{\rm att}$ and $\mathcal{I}^{R}_{\rm att}$ in (17) and (18). The differences arise near the probe-to-patch junction as in Figs. 5 and 6, evidenced by the presence of the discontinuity in Fig. 5. Similar remarks apply to the results for the y component in Figs. 9–12.

The results indicate that while there may not be precise point-wise agreement between the eigenfunction and residue series, satisfactory global agreement between $\Phi^{xE}_{\rm att}(x, y)$ and $\Phi^{xR}_{\rm att}(x, y)$ exists over the entire patch area. (The same is true for the y component of the attachment mode.) This global nature of the agreement allows one to conclude that one may expect smaller relative errors defined by (16).

It must be emphasized that such close agreement is only possible for integration in the space domain. In the spectral domain, where the entries of the impedance matrix are improper integrals [10], [11], this agreement cannot be expected. The reason is that in the spatial domain the iterated integrations in (17) and (18) can be interpreted as area intercepted under a curve. The discontinuity shown in Figs. 5 and 9, at the probe-to-patch junction, is a very small fraction of the total area of the entire support region. This feature, in the spatial domain integration, provides closer

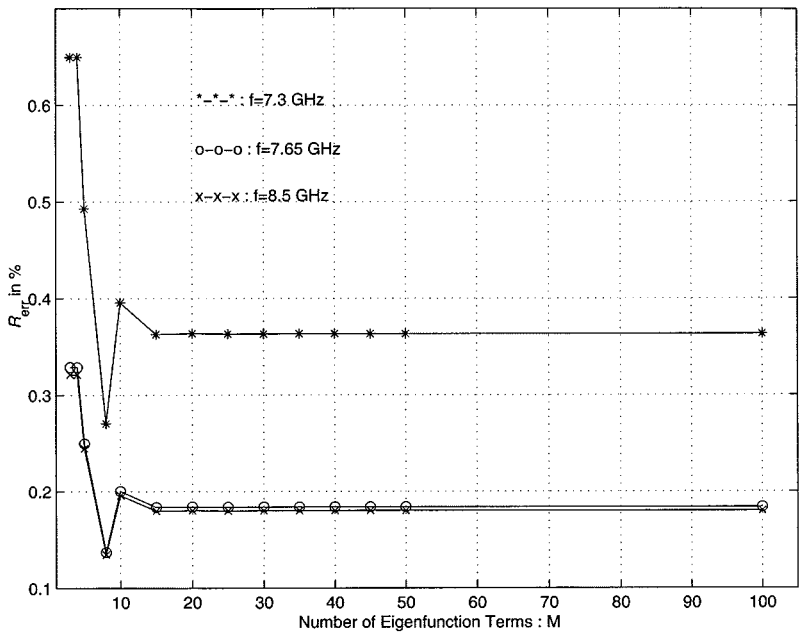

Fig. 15. Frequency dependence of $\mathcal{R}_{\rm crr}$ for the x component of the attachment mode using two terms of the residue series in each case.

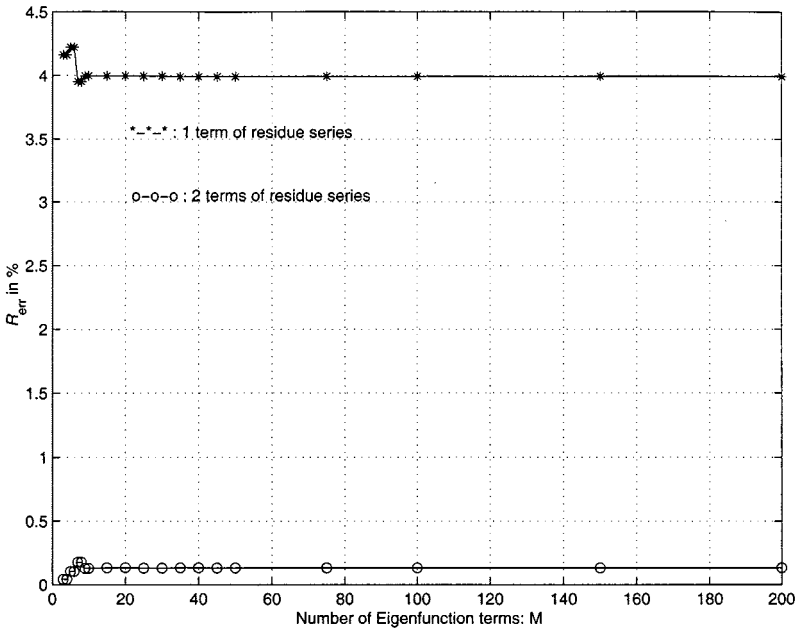

Fig. 16. Comparisons of $\mathcal{R}_{\rm crr}$ for the y component of the attachment mode at $f = 8.5$ GHz.

numerical agreement between (17) and (18) for both components and forms of the attachment mode.

In contrast, the spectral-domain method [3] consists of evaluating of Fourier transforms of the relevant expansion functions over the finite area of the patch. The Fourier transforms of the residue and eigenfunction series for the attachment mode are not the same because the transform of the function modeling the probe-to-patch discontinuity occupies the entire wavenumber spectrum and, hence, is a dominant part of the complete spectral representation of the attachment mode.

The global characteristics of the results in Figs. 5–12 help explain the nature of the convergence properties of the two different forms for the attachment mode. The results in Figs. 13–18 demonstrate the superior convergence properties of the residue series ($(\Phi_{\rm att}^{xR}(x,y)$ and $\Phi_{\rm att}^{yR}(x,y)$) forms for the expansion functions. These results are briefly discussed below.

In Fig. 13, the $\mathcal{R}_{\rm err}$ is computed via (16)–(18) for the x component of the attachment mode and for its one- and two-term residue series representations. The results show that $\mathcal{R}_{\rm err}$ stabilizes only when $M \geq 20$. The approximate cpu times for the two cases are shown in Fig. 14. The individual cpu times for the one- and two-term evaluation of (18) are 1.13 and 1.68 s, respectively. One can conclude by examining these figures that the best representation of the attachment mode-expansion function

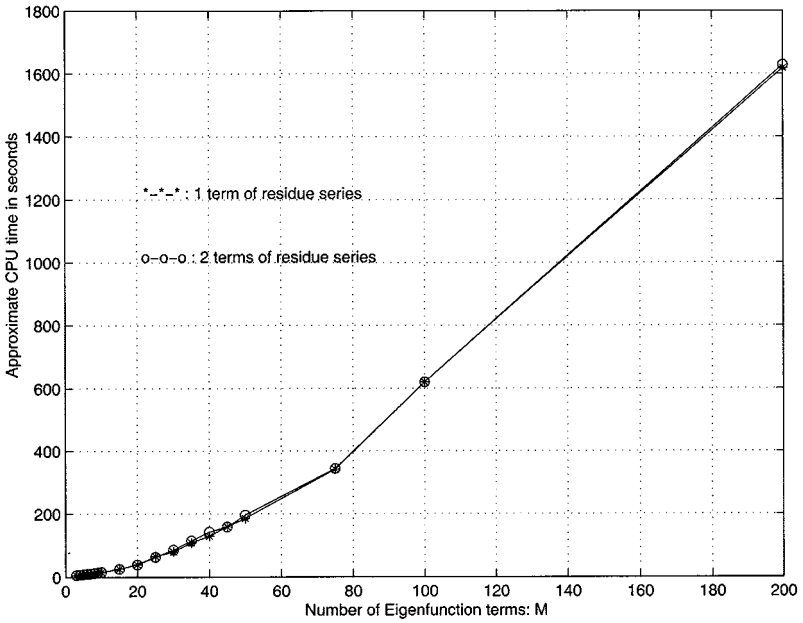

Fig. 17. Computation cost for the y component of the eigenfunction series for the attachment mode at $f = 8.5$ GHz.

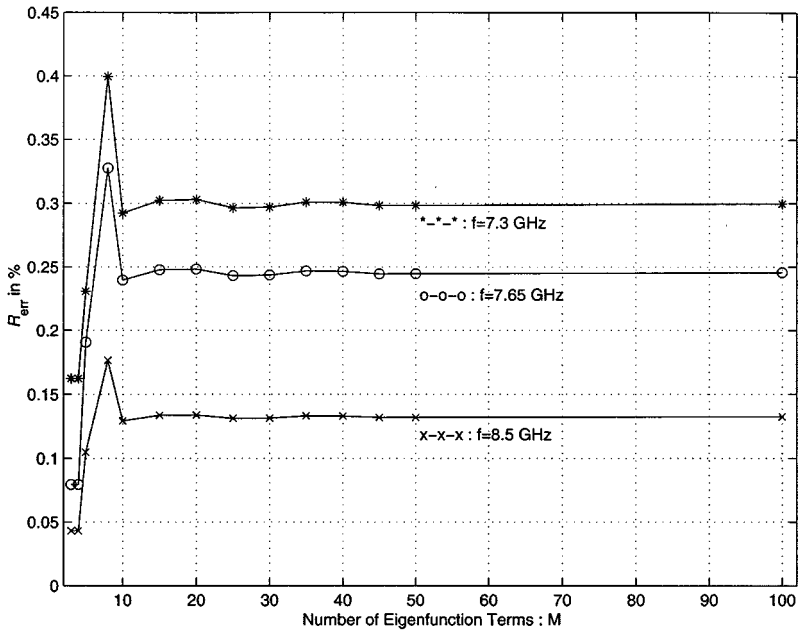

Fig. 18. Frequency dependence of $\mathcal{R}_{\rm err}$ for the y component of the attachment mode using two terms of the residue series in each case.

(for space-domain calculations) is obtained when (5) is used. In Fig. 15, the $\mathcal{R}_{\rm err}$ versus M is shown for the complete impedance bandwidth for this patch configuration. It is generally true that over this 16% impedance bandwidth, a two-term residue series representation gives adequate numerical accuracy compared to at least 20 terms of the corresponding eigenfunction series.

Figs. 16–18 exhibit the same nature for the y component of the attachment mode. The individual cpu times for the one- and two-term evaluations of (18) are 1.77 and 2.30 s, respectively. However, one observes by comparing results in Figs. 5 and 16 that a one-term representation for the y component is worse compared to the single-term residue series for the x component. The reason for this can be explained by examining results in Figs. 5, 6 (x-component), 9, and 10 (y-component). It is clear that the real parts for the x-component agree better compared to the y-component for the two-term residue series. The one-term representation of the residue series for the y-component showed far more disagreements with the eigenfunction series shown in Fig. 9. Despite such differences the two-term representation for the y-component gives satisfactory results for $\mathcal{R}_{\rm err}$ for all cases of interest.

In general, the numerical investigations showed that the attachment mode-expansion function for both the x- and y-components can be replaced by their two-term residue series de-

rived earlier [20]. For space-domain calculations, it was found that about 20 eigenfunction terms for each component were numerically adequate compared to their respective two-term residue series. This feature further allows application of an analytical technique to reduce the fourfold reaction integrals to their appropriate twofold representations, thus significantly reducing the $[Z]$ matrix fill time and the overall MoM computation time, respectively, by several orders of magnitude. Similar conclusions were reached for other data in [15]. Additionally, other forms for $\mathcal{U}(x, y)$ in (15) were examined. The nature of these results and, hence, the inferences, were similar to the ones included here.

V. Conclusion

Moment-method characterization of wide-band probe-fed rectangular microstrip arrays and elements requires the inclusion of a probe-to-patch attachment mode-expansion function for accurate prediction of their impedance characteristics. It has been shown in this paper that the infinite eigenfunction series form for this expansion function yields impedance matrix elements that contain terms that are dual infinite series of finite-range fourfold spatial integrals. Such a complicated series form increases the fill time of the impedance matrix and, hence, reduces the efficiency of an MoM analysis. In contrast, it has been shown that the residue series form for the attachment mode contains a finite number of terms involving finite-range fourfold spatial integrals that are far more suitable for computation. Numerical comparisons show that the two-term residue series gives almost the same results that are obtained using at least 15–20 terms of the eigenfunction series. Additionally, results for the cpu time indicate that the cost of computation increases substantially as the number of terms in the eigenfunction series is increased. The analysis showed that a one- or two-term residue series for the attachment mode exhibits superior convergence properties over the eigenfunction series. Furthermore, the residue series can be used in a relatively straightforward manner for analytic reduction of the reaction integrals in the elements of the impedance matrix, from four-dimensional (4-D) to 2-D forms. The numerical analysis of the convergence properties of the attachment mode thus emphasize the development of an efficient space-domain MoM technique for modeling microstrip elements and arrays for a wide variety of applications.

Acknowledgment

One of the authors, D. Chatterjee, would like to thank Profs. R. K. Moore, Black, and Veatch. He would also like to thank Distinguished Professor Emeritus, the Electrical Engineering and Computer Science Department, University of Kansas, for his encouragement during the time this paper was written. The authors would also like to thank D. Graham, Radar Systems and Remote Sensing Laboratory, University of Kansas, Lawrence, for her careful editing of the initial manuscript, M. Hulet and R. Kershenbaum of the Information Telecommunications Technology Center and Academic Computing Services, respectively, University of Kansas for their help in providing computing facilities during the initial phase of this work.

References

[1] R. B. Waterhouse, S. D. Targonski, and D. M. Kotokoff, "Design and performance of small printed antennas," *IEEE Trans. Antennas Propagat.*, vol. 46, pp. 1629–1633, Nov. 1998.

[2] J. F. Zürcher and F. E. Gardiol, *Broadband Patch Antennas*. Norwood, MA: Artech House, 1995.

[3] K. F. Lee and W. Chen, Eds., *Advances in Microstrip and Printed Antennas*. New York: Wiley, 1997.

[4] R. A. Sainati, *CAD of Microstrip Antennas for Wireless Applications*. Norwood, MA: Artech House, 1996.

[5] K. L. Virga and Y. Rahmat-Samii, "Efficient wide-band evaluation of mobile communications antennas using $[Z]$ or $[Y]$ matrix interpolation with method of moments," *IEEE Trans. Antennas Propagat.*, vol. 47, pp. 65–76, Jan. 1999.

[6] R. F. Harrington, *Field Computation by Moment Methods*. New York: IEEE Press, 1993.

[7] E. H. Newman, "An overview of the hybrid MM/Green's function method in electromagnetics," *Proc. IEEE*, vol. 76, pp. 270–282, Mar. 1988.

[8] S. Barkeshli, P. H. Pathak, and M. Marin, "An asymptotic closed-form microstrip surface Green's function for the efficient moment method analysis of mutual coupling in microstrip antennas," *IEEE Trans. Antennas Propagat.*, vol. 38, pp. 1374–1383, Sept. 1990.

[9] K. A. Michalski, "Extrapolation methods for Sommerfeld integral tails," *IEEE Trans. Antennas Propagat.*, vol. 46, pp. 1405–1418, Oct. 1998.

[10] S.-O. Park and C. A. Balanis, "Analytical technique to evaluate the asymptotic part of the impedance matrix of Sommerfeld-type integrals," *IEEE Trans. Antennas Propagat.*, vol. 45, pp. 798–805, May 1997.

[11] S.-O. Park, C. A. Balanis, and C. R. Birchter, "Analytical evaluation of the asymptotic impedance matrix of a grounded dielectric slab with roof-top functions," *IEEE Trans. Antennas Propagat.*, vol. 46, pp. 251–259, Feb. 1998.

[12] R. W. Scharstein, "Mutual coupling in a slotted phased array, infinite in E-plane and finite in H-plane," *IEEE Trans. Antennas Propagat.*, vol. 38, pp. 1186–1191, Aug. 1990.

[13] M. I. Aksun and R. Mittra, "Choices of expansion and testing functions for the method of moments applied to a class of electromagnetic problems," *IEEE Trans. Microwave Theory Tech.*, vol. 41, pp. 503–509, Mar. 1993.

[14] L. Atalan, M. I. Aksun, K. Mahadevan, and M. T. Birand, "Analytical evaluation of the MoM matrix elements," *IEEE Trans. Microwave Theory Tech.*, vol. 44, pp. 519–525, Apr. 1996.

[15] D. H. Schaubert, D. M. Pozar, and A. Adrian, "Effect of microstrip antenna substrate thickness and permittivity: Comparison of theories with experiment," *IEEE Trans. Antennas Propagat.*, vol. 37, pp. 677–683, June 1989.

[16] J. T. Aberle and D. M. Pozar, "Analysis of infinite arrays of probe-fed rectangular microstrip patches," *Proc. Inst. Elect. Eng.*, pt. H, vol. 136, pp. 110–119, Apr. 1989.

[17] D. M. Pozar and E. H. Newman, "Analysis of a monopole mounted near or at the edge of a half-plane," *IEEE Trans. Antennas Propagat.*, vol. AP-29, pp. 488–495, May 1981.

[18] R. K. Moore, *IMSL User's Manual*. Houston, TX: IMSL Customer Support, Aug. 1989, version 1.1.

[19] J. R. Rice, *Numerical Methods, Software, and Analysis*. New York: Academic, 1993.

[20] D. Chatterjee and R. G. Plumb, "A hybrid formulation for the probe-to-patch attachment mode current for rectangular microstrip antennas," *IEEE Trans. Antennas Propagat.*, vol. 44, pp. 677–686, May 1996.

[21] "Convergence considerations in moment-method analysis of a class of microstrip antennas," in *IEEE Antennas Propagat. Symp. Dig.*, vol. 2, Montréal, Québec, Canada, July 1997, pp. 602–605.

[22] D. Chatterjee, "Advances in modeling techniques for a class of microstrip antennas," Ph.D. Dissertation, Dept. of Electrical Engineering and Computer Science, University of Kansas, Lawrence, Kansas, Feb. 1998.

Deb Chatterjee (S'86–M'98) was born in Calcutta, India, in 1959. He received the B.E.Tel.E. degree from Jadavpur University, Calcutta, the M.Tech. degree from IIT Kharagpur, India, the M.A.Sc. (Master of Applied Science) degree from Concordia University, Montreal, Canada, and the Ph.D. degree from University of Kansas, Lawrence, Kansas, in 1981, 1983, 1992, and 1998, respectively, all in electrical engineering.

From 1983 to 1986, he was employed at the Antenna Group, Radar Division at the Avionics and Design Bureau at Hindustan Aeronautics Limited (HAL), Hyderabad, India, as an Antenna Engineer, where he was involved in numerical analysis and modeling of waveguide and horn antenna feeds for monopulse radars. From 1992 to 1998 he was a Graduate Research Assistant and later a Lecturer with the Electrical Engineering and Computer Science Department, University of Kansas. During this time he had worked on topics related to modeling of microstrip antennas and scattering from dielectric particles, with applications to wireless communications and spaceborne scatterometry, respectively. From 1998 to 1999 he was a Postdoctoral Research Engineer at the University of Kansas. In August 1999 he accepted the tenure-track position of an Assistant Professor at the University of Missouri-Columbia's Coordinated Engineering Program, Kansas City. His major research interests are in analytical and computational electromagnetics, microstrip antennas for wireless applications, inverse electromagnetic scattering for biomedical applications and the like.

Richard G. Plumb (S'82–M'88–SM'94) was born in Syracuse, NY, in 1959. He received the B.S., M.S., and Ph.D. degrees in electrical engineering from Syracuse University, NY, in 1982, 1985, and 1988, respectively.

From 1982 to 1986, he worked at General Electric, Syracuse, NY. In 1985, he completed General Electric's Advanced Course in Engineering. Between 1986 and 1988, he was a Graduate Research Assistant at Syracuse University, and for the 1988 academic year, he was a Visiting Assistant Professor. In 1989 he joined the faculty in the Department of Electrical Engineering and Computer Science, the University of Kansas, Lawrence, Kansas. During 1996 he was a Visiting Scholar at the University of Queensland, Brisbane, Australia. In 1998 he joined the Electrical Engineering Department, State University of New York at Binghamton, where he is currently Professor and Chair. His primary research interests are in electromagnetics, ground-penetrating radar, and inverse scattering.